An early modern human presence in Sumatra 73,000–63,000 years ago

K. E. Westaway, J. Louys, R. Due Awe, M. J. Morwood, G. J. Price, J.-x. Zhao, M. Aubert, R. Joannes-Boyau, T. M. Smith, M. M. Skinner, T. Compton, R. M. Bailey, G. D. van den Bergh, J. de Vos, A. W. G. Pike, C. Stringer, E. W. Saptomo, Y. Rizal, J. Zaim, W. D. Santoso, A. Trihascaryo, L. Kinsley & B. Sulistyanto

LETTER

doi:10.1038/nature23452

An early modern human presence in Sumatra 73,000–63,000 years ago

K. E. Westaway[1], J. Louys[2], R. Due Awe[3]‡, M. J. Morwood[4]‡, G. J. Price[5], J.-x. Zhao[5], M. Aubert[6], R. Joannes-Boyau[7], T. M. Smith[8,9], M. M. Skinner[10,11], T. Compton[12], R. M. Bailey[13], G. D. van den Bergh[4], J. de Vos[14], A. W. G. Pike[15], C. Stringer[12], E. W. Saptomo[3], Y. Rizal[16], J. Zaim[16], W. D. Santoso[16], A. Trihascaryo[16], L. Kinsley[17] & B. Sulistyanto[3]

Genetic evidence for anatomically modern humans (AMH) out of Africa before 75 thousand years ago (ka)[1] and in island southeast Asia (ISEA) before 60 ka (93–61 ka)[2] predates accepted archaeological records of occupation in the region[3]. Claims that AMH arrived in ISEA before 60 ka (ref. 4) have been supported only by equivocal[5] or non-skeletal evidence[6]. AMH evidence from this period is rare and lacks robust chronologies owing to a lack of direct dating applications[7], poor preservation and/or excavation strategies[8] and questionable taxonomic identifications[9]. Lida Ajer is a Sumatran Pleistocene cave with a rich rainforest fauna associated with fossil human teeth[7,10]. The importance of the site is unclear owing to unsupported taxonomic identification of these fossils and uncertainties regarding the age of the deposit, therefore it is rarely considered in models of human dispersal. Here we reinvestigate Lida Ajer to identify the teeth confidently and establish a robust chronology using an integrated dating approach. Using enamel–dentine junction morphology, enamel thickness and comparative morphology, we show that the teeth are unequivocally AMH. Luminescence and uranium-series techniques applied to bone-bearing sediments and speleothems, and coupled uranium-series and electron spin resonance dating of mammalian teeth, place modern humans in Sumatra between 73 and 63 ka. This age is consistent with biostratigraphic estimations[7], palaeoclimate and sea-level reconstructions, and genetic evidence for a pre-60 ka arrival of AMH into ISEA[2]. Lida Ajer represents, to our knowledge, the earliest evidence of rainforest occupation by AMH, and underscores the importance of reassessing the timing and environmental context of the dispersal of modern humans out of Africa.

Lida Ajer is a small multi-chambered cave in the Padang Highlands situated to the south of Payakumbuh village, west Sumatra (Fig. 1 and Extended Data Fig. 1). A rear chamber (Fig. 1c) was excavated by Dubois between 1887 and 1890 (ref. 10), which contains a rich fossiliferous breccia (Fig. 2) that preserves a rainforest fauna[7,11] (Extended Data Fig. 2). Two hominin teeth recovered from the deposit, an upper central incisor and second molar (Fig. 3d 1, 2 and Extended Data Fig. 3), were classified as human based on their size and morphology[12]. Despite the potential importance of these finds, the age of the site is unconfirmed owing to an estimated age of 90–60 thousand years (kyr) on the basis of biochronology[11] and relative age of >81 kyr using amino acid racemization (AAR) on bone (ref. 13 and R. Skelton, unpublished report).

Lida Ajer is one of a group of sites referred to as the Sumatran or Padang Caves. They also include Sibrambang and Djamboe[11] (both dated to >70 ka by AAR on bone[13]) in addition to numerous unnamed caves excavated by Dubois in the Padang Highlands. Large numbers of orangutan fossils and other closed forest taxa have been recovered from these sites (Extended Data Fig. 2 and Supplementary Table 2), indicative of widespread humid rainforest environments in west Sumatra during the Late Pleistocene[11,12,14]. Owing to many similarities, the Sumatran faunas are considered contemporary with Punung from east Java (128–118 ka (ref. 15))[11,14]. The cave faunas from Sumatra and Java are considered to be intermediate in age between Ngandong and Wadjak (dated to 558–126 ka (ref. 16) and 37–29 ka (ref. 17), respectively; Extended Data Fig. 1b and Supplementary Table 1) and may date to the penultimate interglacial period (around 130–80 ka)[11].

The fossil chamber in Lida Ajer comprises four areas of lithified deposits (Fig. 2). Each area consists of cemented breccias outcropping at the same topographic level, with large, allogenic angular clasts and fossils buried in a clay-rich matrix, overlain and underlain by flowstones. The individual deposits most likely represent the remains of a single, thick sedimentary unit that has since partially eroded, the maximum height of which is represented by the base of the calcite columns in area 3 (Fig. 2b). The majority of species recovered during recent fieldwork (Extended Data Fig. 2) were also recorded by Dubois (Supplementary Table 2), although no additional hominin remains or archaeology were observed in the cave.

The Lida Ajer teeth are smaller than fossil orangutans and east and southeast Asian *Homo erectus*/archaic *Homo sapiens* (Extended Data Fig. 3). They show greater affinity to east Asian Late Pleistocene *H. sapiens* than to southeast Asian Late Pleistocene to mid Holocene *H. sapiens* (Supplementary Tables 3, 4). The relative enamel thickness of the incisor is most similar to mean values for modern humans, and exceeds the extant orangutan range (Extended Data Fig. 4 and Supplementary Table 5). Relative enamel thickness of the molar is intermediate between mean values of living humans and living and fossil orangutans. Discriminant function analysis of molar enamel–dentine junction morphology classifies it as *H. sapiens* (Extended Data Figs 4–6). Both teeth have a simple external morphology typical of *H. sapiens*. They lack traits that characterize east and southeast Asian *H. erectus*/archaic *H. sapiens* and *Homo floresiensis*. Furthermore, derived *H. sapiens* features are found in both teeth, such as incisor double shovelling (Supplementary Information). The combination of their small size and external and internal morphology demonstrates that they are anatomically modern *Homo sapiens*.

[1]Department of Environmental Sciences, Faculty of Science and Engineering, Macquarie University, Sydney, New South Wales 2109, Australia. [2]School of Culture, History, and Languages, ANU College of Asia and the Pacific, Australian National University, Canberra, Australia. [3]Indonesian Centre for Archaeology, Jl. Raya Condet Pejaten No. 4, Jakarta 12001, Indonesia. [4]Centre for Archaeological Sciences, School of Earth and Environmental Sciences, University of Wollongong, Wollongong, New South Wales 2522, Australia. [5]School of Earth and Environmental Sciences, University of Queensland, Brisbane, Queensland 4072, Australia. [6]Place, Evolution and Rock Art Heritage Unit (PERAHU), Griffith University, Gold Coast, Queensland 4222, Australia. [7]Southern Cross GeoScience, Southern Cross University, Military Road, Lismore, New South Wales 2480, Australia. [8]Australian Research Centre for Human Evolution, Environmental Futures Research Institute, Griffith University, 170 Kessels Road, Nathan, Queensland 4111, Australia. [9]Department of Human Evolutionary Biology, Harvard University, 11 Divinity Avenue, Cambridge, Massachusetts 02138, USA. [10]School of Anthropology and Conservation, University of Kent, Canterbury CT2 7NR, UK. [11]Department of Human Evolution, Max Planck Institute for Evolutionary Anthropology, Deutscher Platz 6, Leipzig 04103, Germany. [12]Department of Earth Sciences, Natural History Museum, Cromwell Road, London SW7 5BD, UK. [13]School of Geography and the Environment, University of Oxford, Oxford OX1 2JD, UK. [14]Department of Geology, Naturalis Biodiversity Center, Leiden, The Netherlands. [15]Department of Archaeology, University of Southampton, Highfield Road, Southampton SO17 1BF, UK. [16]Geology Study Program, Institut Teknologi Bandung, Java, Indonesia. [17]Research School of Earth Sciences, Australian National University, Canberra, Australia.
‡Deceased.

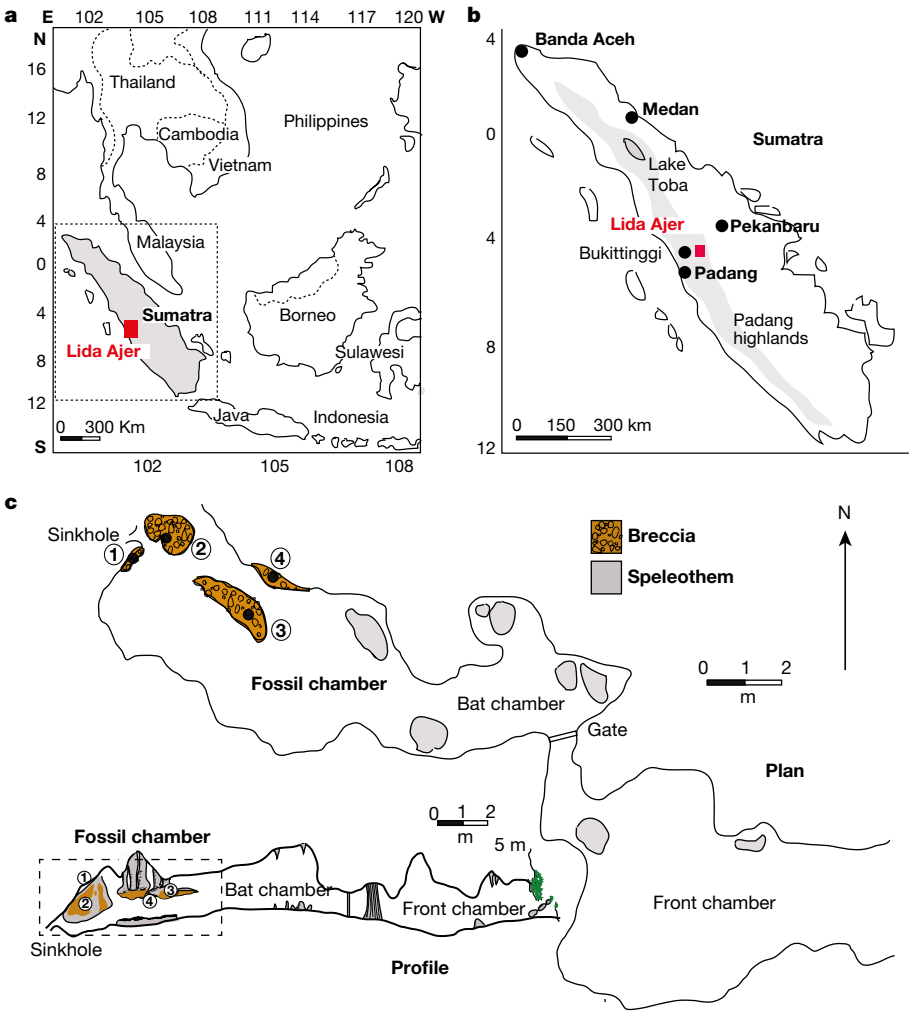

Figure 1 | Location of Indonesia, Sumatra and Lida Ajer cave and associated breccia. **a**, Southeast Asia illustrating the location of Sumatra (redrawn with permission from ref. 7). **b**, Sumatra island illustrating the location of Lida Ajer, close to the volcanic Bukit Barisan Mountains, in the belt of Carboniferous limestone. **c**, Cave plan and profile of Lida Ajer with its three chambers—front, bat and fossil chambers and the four sampling locations. The fossil-bearing breccia unit has been marked in brown with associated speleothem (flowstones, stalagmites and stalactites) marked in grey. The sampling locations—areas 1–4—are indicated on the plan and on the profile.

We used a multidisciplinary dating approach to determine the age of the breccia. Red thermoluminescence and post-infrared infrared-stimulated luminescence (pIR-IRSL) dating of the sediments provided burial ages, while uranium-series (U-series) dating of associated speleothems yielded bracketing ages (Fig. 2). Several fossil teeth of *Pongo* and siamang gibbon were also directly dated using a combination of U-series profiling and coupled U-series/electron spin resonance (U-series/ESR) dating. Those samples included new fossils recovered during our excavations, as well a specimen collected by Dubois[10] (Extended Data Fig. 8d). The resulting age estimates (Supplementary Tables 7, 8, 11) have been summarized in a composite stratigraphic figure (Fig. 3b, c). Technical considerations associated with dating the breccia matrix, fossil teeth and calcite are discussed in the Supplementary Information.

Maximum ages for the deposition of the breccia are constrained by the ^{230}Th age of a basal flowstone of 203 ± 17 kyr (LA-F3) and a straw stalactite dated to 84 ± 1 ka (LA-08-29) that was recovered from the breccia itself. Straw stalactites with large diameters and thin walls (as in this study) precipitate, detach and drop into the underlying sediment over relatively short timescales, and therefore commonly represent ages close to the true time of sedimentary deposition[18]. A minimum age of the fossil breccia is constrained by ^{230}Th ages of overlying flowstones of 71 ± 7 kyr (LA-F1) and 11 ± 2 kyr (LA-F2). Therefore, U-series dating of bracketing speleothems suggests that deposition of the fossils occurred between 84 ± 1 and 71 ± 7 ka. Luminescence dating of the breccia supports this chronology with red thermoluminescence dating suggesting that the quartz grains were last exposed to daylight 85 ± 25 ka (maximum age), while single-aliquot dating of feldspars using pIR-IRSL yielded an age of 62 ± 5 kyr, which probably lies closer to the true age of the breccia deposition[19] (Extended Data Fig. 7 and Supplementary Table 7). Direct dating of fossils yielded minimum ^{230}Th ages of >80–75 kyr (7-, 12-, 13-, 21/LA/5/08, with the tooth (9967A) discovered by Dubois dated to around 70–60 ka, see Supplementary Information) (Extended Data Fig. 8) and coupled U-series/ESR ages of 76 ± 7 kyr and 86 ± 13 kyr (12- and 13/LA/5/08, Extended Data Fig. 9). The results from each independent dating method are in stratigraphic agreement (Fig. 3b).

All chronological data were modelled in a modified Bayesian framework designed to take into account the minimum–maximum range, true age or burial age limitations of each age estimate. This provides the best estimate for the burial age and, to our knowledge, the first numerical age for the Lida Ajer fauna of 68 ± 5 kyr (mean ± 1σ; age range, 73–63 kyr) (Fig. 3c and Extended Data Fig. 10). This is broadly in agreement with the previous AAR estimations[13], regional biostratigraphic correlations[11] and regional sea-level reconstructions[20], enabling the appearance of a modern rainforest community in Sumatra during a period of connection to other Sunda landmasses.

The presence of modern humans in Sumatra between 73 and 63 ka is substantially earlier (around 20 ka, for example, ref. 21) than previous skeletal records in ISEA, but is consistent with new evidence for a human presence in northern Laos 70–46 ka (ref. 22), with genetics-based estimates of AMH presence in Asia before the Younger Toba Eruption[3] (although recent recalibration places this at 71.6 ka (ref. 23)), and with stone-tool evidence from Asia[24]. This minimum arrival date also agrees with a prediction using analysis of mitochondrial DNA that AMH were in southeast Asia 79–75 ka (ref. 2). While

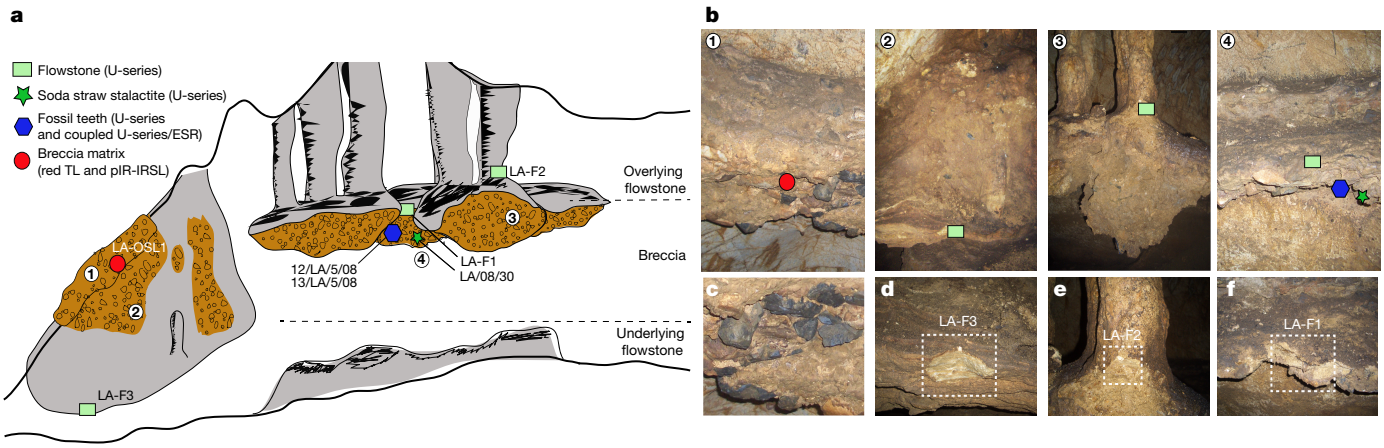

Figure 2 | Lida Ajer breccia; structure and stratigraphic relationships. **a**, An enlargement of the fossil chamber in Fig. 1c (dashed box) demonstrating the stratigraphic relationships and locations of samples that were collected for U-series dating of the flowstones (rectangles) and soda straw (star), U-series and coupled U-series/ESR of the fossil teeth (hexagon), and red thermoluminescence (TL) and pIR-IRSL of the breccia matrix (circle). **b**, The four main areas of breccia in the cave depicted by photographs. Areas 1–4 correlate with the marked sampling areas in **a**, and the symbols refer to the dating techniques listed in the key. **c**, The breccia from area 1 showing the angular clasts and sandy clay matrix. **d**, The underlying flowstone from area 2 was sampled for U-series dating (LA-F3). **e**, The calcite column from area 3 was sampled for U-series dating (LA-F2). **f**, The overlying flowstone from area 4 was sampled for U-series dating (LA-F1).

it is at odds with popular estimates of a marine oxygen isotope stage 4 (MIS4, between 74 and 58 ka) exit from Africa[3], it supports more recent lines of evidence that argue for an earlier exit from Africa[25].

The presence of a closed canopy rainforest ecosystem in Sumatra 73–63 ka is supported by pre-Toba pollen evidence from off-shore north Sumatra[26], as well as broad-scale palaeoenvironmental reconstructions of Pleistocene rainforest persistence in western Sumatra[14,27] (Fig. 1a). Notably, our results provide the earliest unambiguous evidence of occupation of rainforest conditions by AMH. The longstanding preferred route of modern humans out of Africa has been along a 'coastal dispersal corridor'[28], which is thought to have occurred during MIS4 when many Asian environments were considered inhospitable to early AMH. Marine environments offer particularly favourable conditions for human subsistence and movement. Conversely, rainforests, with their highly spaced, seasonal resources, scarce fat-rich faunas and dearth of carbohydrate-rich plants[29], present serious difficulties for movement and colonization by hominins that evolved in open environments. Successful exploitation of rainforest environments requires the capacity for complex planning and technological innovations: the behavioural hallmark of our species. Our data indicate that such innovations and capacities were in place in Asia well before MIS4. Furthermore, the presence of modern humans in the Padang Highlands indicates that humans were able to disperse beyond the coast when or shortly after arriving in southeast Asia.

This new chronology for modern human arrival in Indonesia supports calls for a reassessment of the timing and environmental context of human movement out of Africa. An age of 73–63 kyr is consistent with mitochondrial DNA predictions[2] and emerging palaeoanthropological data from the broader region[22]. Our study provides unique insights into the chronological and environmental framework of dispersals through the region. Most importantly, we suggest that behavioural flexibility and technological innovations that are required

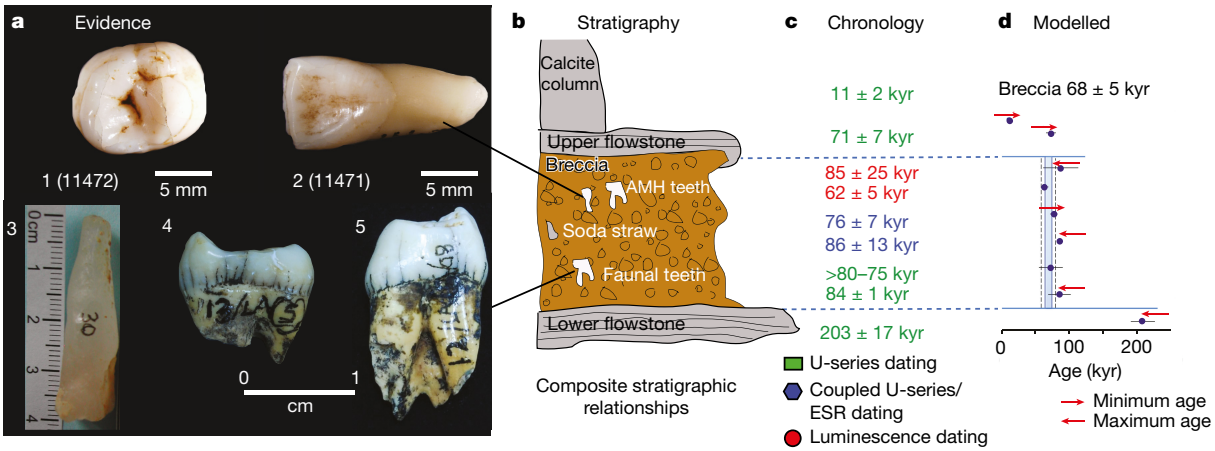

Figure 3 | A summary of the results from the Lida Ajer cave analysis. **a**, The associated evidence: 1, 2, the human teeth from Lida Ajer discovered by Dubois and first identified by Hooijer (see Extended Data Fig. 3e, f for the full version); 3, the soda straw stalactite discovered in the cave breccia and used for dating; 4, 5, *Pongo* sp. fossil molar teeth used for U-series and coupled U-series/ESR dating (13- and 12/LA/5/08) (Extended Data Figs 8, 9). **b**, A composite stratigraphy of the cave to simplify the stratigraphic relationships and associations with the fossil material. **c**, The new chronology for Lida Ajer using multiple dating techniques (red thermoluminescence (red), U-series thermal ionization mass spectrometry (TIMS) (green) and U-series multi-collector inductively coupled mass spectrometry (MC-ICPMS) profiling and coupled U-series/ESR. Results are colour coded for each technique). Note: the red thermoluminescence and ESR error of the age estimates are presented at 1σ, whereas the U-series errors have been presented at 2σ. **d**, The dating results modelled to constrain the age of the breccia to 68 ± 5 kyr (73–63 kyr).

for successful utilization of complex and challenging environments, as seen in other caves in the region[21], were in place by the beginning of MIS4. Such traits were no doubt instrumental in precipitating the successful migration of modern humans out of Africa.

Online Content Methods, along with any additional Extended Data display items and Source Data, are available in the online version of the paper; references unique to these sections appear only in the online paper.

Received 30 March; accepted 29 June 2017.
Published online 9 August 2017.

1. Pagani, L. *et al.* Genomic analyses inform on migration events during the peopling of Eurasia. *Nature* **538,** 238–242 (2016).
2. Fu, Q. *et al.* A revised timescale for human evolution based on ancient mitochondrial genomes. *Curr. Biol.* **23,** 553–559 (2013).
3. Oppenheimer, S. The great arc of dispersal of modern humans: Africa to Australia. *Quat. Int.* **202,** 2–13 (2009).
4. Dennell, R. & Petraglia, M. D. The dispersal of *Homo sapiens* across southern Asia: how early, how often, how complex? *Quat. Sci. Rev.* **47,** 15–22 (2012).
5. Liu, W. *et al.* The earliest unequivocally modern humans in southern China. *Nature* **526,** 696–699 (2015).
6. Morwood, M. J. *et al.* Climate, people and faunal succession on Java, Indonesia: evidence from Song Gupuh. *J. Archaeol. Sci.* **35,** 1776–1789 (2008).
7. de Vos, J. in *The Encyclopedia of Quaternary Science* (ed. Elias, S. A.) 3232–3249 (Elsevier, 2007).
8. Morwood, M. J. *et al.* Preface: research at Liang Bua, Flores, Indonesia. *J. Hum. Evol.* **57,** 437–449 (2009).
9. Schwartz, J. H., Long, V. T., Cuong, N. L. Kha, L. T. & Tattersall, I. A review of the Pleistocene hominoid fauna of the Socialist Republic of Vietnam (excluding Hylobatidae). *Anthropol. Pap. Am. Mus. Nat. Hist.* **76,** 1–24 (1995).
10. Dubois, E. Voorlopig bericht omtrent het onderzoek naar de Pleistocene en Tertiaire vertebraten-fauna van Sumatra en Java, gedurende het jaar 1890. *Nat. Tijdschr. Ned. Indië* **51,** 93–100 (1891).
11. de Vos, J. The *Pongo* faunas from Java and Sumatra and their significance for biostratigraphical and paleo-ecological interpretations. *Proc. Koninklijke Nederlandse Akademie Wetenschappen* **86,** 417–425 (1983).
12. Hooijer, D. A. Prehistoric teeth of man and of the orang-utan from central Sumatra, with notes on the fossil orang-utan from Java and Southern China. *Zool. Meded.* **29,** 175–301 (1948).
13. Drawhorn, G. M. *The Systematics and Paleodemography of Fossil Orangutans*. PhD Thesis, Univ. California (Davis, 1994).
14. Louys, J. & Meijaard, E. Palaeoecology of southeast Asian megafauna-bearing sites from the Pleistocene and a review of environmental changes in the region. *J. Biogeogr.* **37,** 1432–1449 (2010).
15. Westaway, K. E. *et al.* Age and biostratigraphic significance of the Punung rainforest fauna, East Java, Indonesia; implications for *Pongo* and *Homo*. *J. Hum. Evol.* **53,** 709–717 (2007).
16. Indriati, E. *et al.* The age of the 20 meter Solo River terrace, Java, Indonesia and the survival of *Homo erectus* in Asia. *PLoS ONE* **6,** e21562 (2011).
17. Storm, P. *et al.* U-series and radiocarbon analyses of human and faunal remains from Wajak, Indonesia. *J. Hum. Evol.* **64,** 356–365 (2013).
18. St Pierre, E. J. *et al.* Preliminary U-series and thermoluminescence dating of deposits in Liang Bua sub-chamber, Flores, Indonesia. *J. Archaeol. Sci.* **40,** 148–155 (2013).
19. Roberts, R. G. *et al.* Geochronology of cave deposits in Liang Bua and of adjacent river terraces in the Wae Racang valley, western Flores, Indonesi: a synthesis of age estimates for the type locality of *Homo floresiensis*. *J. Hum. Evol.* **57,** 484–502 (2009).
20. Louys, J. & Turner, A. Environment, preferred habitats and potential refugia for Pleistocene *Homo* in Southeast Asia. *C. R. Palevol* **11,** 203–211 (2012).
21. Barker, G. & Farr, L. (eds) *Archaeological Investigations in the Niah Caves, Sarawak, 1954–2004* Monographs 2 (McDonald Institute for Archaeological Research, 2016).
22. Shackelford, L. *et al.* Additional evidence for early modern human morphological diversity in Southeast Asia at Tam Pa Ling, Laos. *Quat. Int.* https://doi.org/10.1016/j.quaint.2016.12.002 (in the press) (2017).
23. Oppenheimer, S. A single southern exit of modern humans from Africa: before or after Toba? *Quat. Int.* **258,** 88–99 (2012).
24. Petraglia, M. D., Ditchfield, P., Jones, S., Korisettar, R. & Pal, J. N. The Toba volcanic super-eruption, environmental change, and hominin occupation history in India over the last 140,000 years. *Quat. Int.* **258,** 119–134 (2012).
25. Groucutt, H. S. *et al.* Rethinking the dispersal of *Homo sapiens* out of Africa. *Evol. Anthropol.* **24,** 149–164 (2015).
26. van der Kaars, S. *et al.* The influence of the ~73 ka Toba super-eruption on the ecosystems of northern Sumatra as recorded in marine core BAR94-25. *Quat. Int.* **258,** 45–53 (2012).
27. Newsome, J. & Flenley, J. R. Late Quaternary vegetational history of the Central Highlands of Sumatra. II. Palaeopalynology and vegetational history. *J. Biogeogr.* **15,** 555–578 (1988).
28. Erlandson, J. M. & Braje T. J. Coasting out of Africa: the potential of mangrove forests and marine habitats to facilitate human coastal expansion via the Southern Dispersal Route. *Quat. Int.* **382,** 31–41 (2015).
29. Roberts, P. & Petraglia, M. Pleistocene rainforests: barriers or attractive environments for early human foragers? *World Archaeol.* **47,** 718–739 (2015).

Supplementary Information is available in the online version of the paper.

Acknowledgements This research was funded by Australian Research Council Discovery grants (DP1093049, DP140100919, and DP120101752 to K.E.W., R.J.-B., and G.J.P. *et al.*, respectively) and a Leaky Foundation grant and Research School of Asia and the Pacific Grant Development Support grant to J.L. C.S.'s research is supported by the Human Origins Research Fund and the Calleva Foundation. We acknowledge the Max Planck Society for funding micro-CT scanning of the teeth, A. Olejnicak and J. P. Zermeno for assistance with section preparation, and support provided by the Centre from Archaeology in Padang Sumatra and ARKENAS in Jakarta and for allowing access to the site and four fossil faunal teeth for dating. We thank the Department of Geology, Naturalis Biodiversity Center in Leiden, The Netherlands for providing access to Dubois's fieldnote book, excavation details, the two modern human teeth for scanning and the *Pongo* tooth for dating, and we thank C. Bronk Ramsey for assistance with age modelling.

Author Contributions K.E.W., R.D.A., J.L., G.J.P., W.D.S. mapped and excavated the site and collected faunal and dating samples, K.E.W. conducted the red thermoluminescence and pIR-IRSL dating, J.-x.Z. and G.J.P. conducted the U-series measurements on the speleothem, while M.A. and L.K. conducted U-series profiling on the fossil teeth and R.J.-B. conducted the U-series/ESR dating. G.D.v.d.B. and R.D.A. analysed the fauna and M.J.M., G.D.v.d.B., J.d.V., Y.R., J.Z., W.D.S. and A.T. helped to find and organize access to the site. T.M.S. and J.d.V. conducted the micro-CT scanning of the teeth, and T.M.S. measured enamel thickness. T.C. and C.S. described the teeth and M.M.S. analysed the enamel–dentine junction. R.M.B. aided in the design of the dating approach and conducted the Bayesian modelling, while A.W.G.P. conducted the modelling of the U-series age estimates. Finally, E.W.S. and B.S. helped with the dating of the fauna and K.E.W., J.L., G.J.P., J.-x.Z., R.J.-B., G.D.v.d.B., M.A., T.M.S., T.C., M.M.S., C.S. and J.d.V. wrote the paper, with early contributions from M.J.M. and R.D.A.

Author Information Reprints and permissions information is available at www.nature.com/reprints. The authors declare no competing financial interests. Readers are welcome to comment on the online version of the paper. Publisher's note: Springer Nature remains neutral with regard to jurisdictional claims in published maps and institutional affiliations. Correspondence and requests for materials should be addressed to K.E.W. (kira.westaway@mq.edu.au).

Reviewer Information *Nature* thanks G. Barker, R. Dennell and the other anonymous reviewer(s) for their contribution to the peer review of this work.

METHODS

Tooth morphology and metrics. Measurements of the Lida Ajer teeth are taken from ref. 12 and, for the root robusticity and crown height of the M^2, measured from photographs scaled using the crown measurements (Extended Data Fig. 3). For the latter, root robusticity was measured using the method described in ref. 30 and crown height using the method described in ref. 31. Relative cusp areas of the molar were measured from a photograph of the occlusal surface using ImageJ software (Rasband, 1997–2008)[32]. The grade numbers referred to in the following sections are those defined in the Arizona State University Dental Anthropology System using their dental plaques[33].

Micro-CT relative enamel thickness. We applied microcomputed tomographic (micro-CT) imaging to assess the relative enamel thickness of the teeth (Extended Data Fig. 4). The teeth were scanned with a Skyscan 1172 micro-CT, and virtual section planes were cut along the labio-lingual aspect of the incisor (11471) and across the mesial cusps of the molar (11472) following established protocols[34–36]. Several variables were quantified on 2D section planes with Sigma Scan Pro software interfaced to a Wacom digitizing tablet following refs 37, 38, enamel cap area (c), enamel–dentine junction (EDJ) length (e), and coronal dentine area enclosed by the enamel cap (b). Average enamel thickness was calculated as c / e, yielding the average straight-line distance (mm units), or thickness, from the EDJ to the outer enamel surface. Average enamel thickness was scaled for comparisons between taxa of different size by calculation of relative enamel thickness: $100\left(\frac{c/e}{\sqrt{b}}\right)$ (Supplementary Table 5).

Micro-CT of the EDJ. We followed a similar methodological approach as described in refs 39, 40. In brief, each molar was micro-CT scanned at the Max Planck Institute for Evolutionary Anthropology in Leipzig, Germany, using either an industrial or desktop micro-CT system with a resultant voxel resolution ranging from 14 to 70 μm. The image stacks of each tooth were filtered (using a computer-programmed macro that uses a 3D median and mean-of-least-variance filter) to improve tissue grayscale homogeneity and then manually segmented into enamel and dentine components using Avizo (v.6.1). The EDJ of each molar was extracted as a digital surface model (.ply format).

The EDJ surface models were imported into Avizo for the collection of three sets of 3D anatomical landmarks (Extended Data Fig. 4b). The first set (referred to as 'main') included four landmarks: one on the tip of the dentine horn of each primary cusp. The second set includes landmarks (50–70) along the tops of the ridges that connect the four dentine horns. This set of points forms a continuous line, beginning at the tip of the protocone and moving in a buccal direction. The third set includes landmarks (around 40) along the cervix of the molar, beginning at the midpoint of the buccal face and continuing in a lingual direction. As the ridge and cervix curves were later resampled (see below), it was not initially necessary that the same number of points were placed along the curve for each specimen. Therefore, the spacing of points was dictated such that they did not touch adjacent neighbours, but was not so far apart as to misrepresent aspects of the curve (as represented in Extended Data Fig. 4b).

The process by which a corresponding set of landmarks and semilandmarks was generated for each specimen is outlined in the Supplementary Information. All data processing was done in Mathematica v.6.0 (http://www.wolfram.com/) using a software routine written by P. Gunz. We performed a principal component analysis in shape and form space on the Procrustes coordinates of each specimen. We then used a cross-validated canonical variates analysis using inclusive sets of 10–24 principal components to determine the taxonomic affinity and molar position of the Lida Ajer molar.

Luminescence dating of quartz and feldspar grains. A bulk sediment sample (laboratory code LA-OSL1) for luminescence dating was collected using red-filtered torch light with additional samples for water content and environmental radioactivity determinations. Quartz grains of 90–125 μm in diameter were processed using standard purification procedures, including a final etch in 40% hydrofluoric acid for 45 min to remove the external alpha-dosed rinds[41]. The LA1 sample yielded very small amounts of quartz, 60 mg, of this around 20 mg was used for aliquots A and B to derive the equivalent dose (D_e) estimates (Supplementary Table 7), leaving only around 40 mg for additional testing. In addition, 90–125 μm feldspar grains were etched in 10% hydrofluoric acid for 40 min. A slightly larger amount of feldspar minerals was recovered than quartz, so tests that are vital to the integrity of the final D_e could be conducted. All luminescence analysis was conducted at the 'Traps' luminescence dating facility at Macquarie University in Sydney, Australia.

In the studied region, the quartz is of volcanic origin, so it requires the use of a DAP red thermoluminescence dating technique[42]. Quartz grains were mounted on stainless-steel discs using silicone oil spray, each large aliquot is composed of around 5,000 grains (around 10 mg). The isothermal red thermoluminescence emissions[43–45] were measured using a red-sensitive photomultiplier tube (Electron Tubes Ltd, 9658B) and cooling tower (LCT50 liquid-cooled thermoelectric housing) with Kopp 2-63 and BG-39 filter combination[42], and laboratory irradiations were conducted using a calibrated $^{90}Sr/^{90}Y$ beta source. D_e values were estimated from the 20–30 s interval of isothermal decay (which was bleachable by >380 nm illumination) using the final 160 s as background. Aliquots were heated to 260 °C at a heating rate of 5 K s^{-1} and then held at 260 °C for 1,000 s to minimize the unwanted thermoluminescence from incandescence.

The ability to recover a known dose[46] was restricted by the small amounts of quartz present (60 mg), as seen in samples from Liang Bua in Flores[47], however, limited dose recovery experiments were conducted on four fresh aliquots. The natural signal was removed using an isothermal measurement (heated to 260 °C and held for 1,000 s), a surrogate dose of 50 Gy, a 1 h bleach in a solar simulator and a second, larger dose (100 Gy) was applied and the surrogate D_e was estimated according to the DAP technique[42]. The surrogate doses for aliquot A and B were recovered to within approximately 10% indicating that the standard 260 °C preheat and isothermal measurement combination are appropriate for these samples. This result agrees with previous dose recovery procedures using DAP on a range of samples[42].

The feldspars in this volcanic region suffer from extreme anomalous fading[47]. To overcome these problems we adopted a modified pIR-IRSL protocol using a 300 °C preheating step and 270 °C IRSL stimulation combination following a standard 50 °C infrared stimulation. pIR-IRSL measurements were conducted on feldspars using infrared (875 nm) light-emitting diodes (LEDs) at 80% power for 250 s and the emissions were detected using Schott BG-39 and Corning 7-59 filters to transmit wavelengths of 320–480 nm. Four procedural tests were applied to small aliquots of around 1,000 grains using the following preheat and infrared stimulation combinations: 250 and 225 °C (refs 48, 49), 280 and 250 °C (ref. 50), 300 and 270 °C (ref. 50), and 320 and 290 °C (refs 51, 52)); (1) A preheat plateau test using three discs; (2) fading tests including a prompt, 1 h and 10 h delay; (3) bleaching tests using one fresh aliquot to determine the amount of residual IRSL after an extended bleach of 4 h in a solar simulator and (4) dose recovery tests using two bleached aliquots (bleached using a solar simulator for 4 h) and a surrogate dose of 200 Gy. From these tests it was determined that the 270 °C stimulation and 300 °C preheat combination provided the flattest preheat plateau, best recovery of the surrogate dose, least fading of the pIR-IRSL signal (g value = 1.7% per decade) and lowest residual value (8 Gy). Subsequently, 24 aliquots were used to conduct a modified SAR regenerative-dose procedure. The resulting D_e values were corrected according to the results of residual dose estimation and anomalous fading tests (using a weighted mean fading rate of $1.7 \pm 0.3\%$ per decade). Owing to the sedimentary context of the cave, we estimated the pIR-IRSL age of each sample using the minimum age model divided by the environmental dose rate.

Measurements of ^{238}U, ^{235}U, ^{232}Th (and their decay products) and ^{40}K were estimated using Geiger–Muller multi-counter beta counting of dried and powdered sediment samples in the laboratory and a portable gamma spectrometer in the field. The corresponding (dry) beta and gamma dose rates were obtained using the conversion factors of ref. 53 and the beta-dose attenuation factors of ref. 54, and an effective internal alpha dose rate of 0.03 Gy kyr^{-1} (ref. 55) and 0.72 Gy kyr^{-1} (refs 56, 57) for the 90–125 μm quartz and feldspar samples, respectively (owing to the radioactive decay of ^{40}K and ^{87}Rb), which were made assuming K ($13 \pm 1\%$ (ref. 56) and Rb (400 ± 100 μg g^{-1} (ref. 57)) concentrations, and these estimations were included in the total dose rate. Cosmic-ray dose rates were estimated from published relationships[58], making allowance for the density and 8-m thickness of the limestone roof above the cave deposit, the geometry of the limestone shielding, the sediment overburden at the sample locality (around 2.45–4.20 m), the altitude (around 600 m above sea level) and geomagnetic latitude and longitude (0° and 100°) of the sampling site. The total dose rate was calculated using a long-term water content of $15 \pm 5\%$, which is close to the measured (field) water content of 16%.

U-series dating of speleothems. Calcite crystals free of any weathered surfaces were extracted from each of the above samples and cleaned ultrasonically to remove as much of the sediment contamination as possible, before they were subjected to chemical treatment and isotopic measurements by mass spectrometry[59]. U-series dating of the speleothem samples was conducted in the Radiogenic Isotope Facility of The University of Queensland using a VG Sector 54 thermal ionization mass spectrometer (TIMS) and a Nu Plasma multi-collector inductively coupled mass spectrometer (MC-ICPMS). Analytical procedures follow ref. 59 and refs 60, 61 for TIMS and MC-ICPMS, respectively. $^{230}Th/^{234}U$ ages were calculated using Isoplot EX 3.75 (ref. 62) and half-lives of 75,690 years (^{230}Th) and 245,250 years (^{234}U)[63].

Laser ablation MC-ICPMS analysis of fossil teeth. We analysed four primate teeth (two *Pongo* sp. and two siamang gibbon) selected from our excavation at Lida Ajer and housed in the collection of the Indonesian National Centre for Archaeology in Jakarta (ARKENAS) (Extended Data Fig. 8a–d). In addition, we analysed a

Pongo sp. tooth from Dubois's original excavation collection (9967A), which is housed in the Naturalis Museum in the Netherlands. The samples were analysed for U-series isotopes at the Research School of Earth Sciences U-series laboratory at the Australian National University, Australia. The teeth were cut using a rotatory tool equipped with a thin (100 μm) diamond saw blade and samples were mounted into Al cups with the cross-section surfaces facing up to the top of the sample holder, corresponding to the focal point of the laser in the sampling cell (Extended Data Fig. 8e–h).

U-series isotopic analyses of the teeth were carried out using a Finnigan MAT Neptune MC-ICPMS equipped with multiple ion counters. Two ion counters were set to masses of 230.1 and 234.1. Faraday cups were set to collect the following masses: 232, 235 and 238. Laser sampling used a Lambda Physik LPFPro ArF excimer laser source which lase at $\lambda = 193$ nm. The laser source is coupled to the Neptune MC-ICPMS instrument through an ANU-designed Helex ablation cell. Details of the instrumentation analysis procedure have been modified from those reported in ref. 64 and are reported in detail in ref. 65.

The analyses were carried out with the laser spot size set to 265 μm using a 5 Hz pulse rate. The samples were initially cleaned for 5 s and ablation pits were measured for 50 s. Analyses were made at regular spacing (typically 2 or 3 mm) along traverses that were computer programmed across regions of interest on cut tooth sections. The analyses made along each transect were bracketed between reference standard analyses to correct for instrument drift.

Semi-quantitative analyses of U and Th concentrations were derived alongside repeated measurements of two standards: SRM NIST-610 glass ($U = 461.5\,\mu g\,g^{-1}$; $Th = 457.2\,\mu g\,g^{-1}$), and rhinoceros tooth dentine from Hexian (sample 1118, see ref. 66). Age estimates were calculated using the Isoplot program[67].

Coupled U-series/ESR dating on fossil teeth. We applied direct ESR dating to two teeth (13/LA/5/08 and 12/LA/5/08) to enable coupled U-series/ESR analysis (ref. 68 and R. Joannes-Boyau & T. Bodin, unpublished report) conducted at the ESR laboratory at the Southern Cross University, Lismore, Australia. From each sample, a fragment of enamel was extracted with the same diamond saw, and stripped from any attached dentine and calculus on the surface. The enamel and dentine were separated and the first 100 μm of the enamel was removed on both sides (the EDJ and the occlusal surface). Both LA-ICPMS (Agilent 7700 and ESI NW213) and LA-MC-ICPMS (Thermo Neptune plus and ESI NW193) analyses were performed directly on the enamel fragment and on the dentine in contact, to estimate the uranium content. U-series analyses were conducted using large rasters on both sides of the enamel fragment and all the way along the dentine from the EDJ to the root canal. The *in situ* dosimetry used for the ESR dating was extracted from the OSL dosimetry conducted at the site (Supplementary Information). Sediment content for U, Th and K was estimated from activity values using ^{238}U: $1\,Bq\,kg^{-1} = 81$ p.p.b.; $^{232}Th = 1\,Bq\,kg^{-1} = 246$ p.p.b.; $^{40}K = 1\,Bq\,kg^{-1} = 0.00323\%$.

ESR dating was performed on a Freiberg MS5000 X-band (2 mW microwave power, 0.1 mT modulation amplitude) with goniometer 1,300 with a 10-degree step, and irradiated with an X-ray source ionization chamber from Freiberg (40 kV at 0.5 mA). The source is a stable X-ray gun Varian VF50 integrated in a homogenized irradiation chamber (designed by Freiberg instruments). The emission consistency was tested on an alanine dosimeter and the dose calibrated against gamma irradiation directly on tooth enamel (fossil and modern, unpublished data). The dose–response curve, which represents the radiation sensitivity and susceptibility of the sample, is extrapolated to cross the *x* axes, indicating the D_e. The dose is described as equivalent, since it is determined using either laboratory gamma or X-ray irradiation, while the actual dose received in nature is the sum of all radiations from multi-energetic emissions of α, β, γ and cosmic rays. Dose–response curves were calculated using the MCDoseE 2.0 program using a Markov Chain Monte-Carlo calculation-fitting algorithm (for more details see ref. 69). For the estimation of the equivalent dose (D_e), each fragment was irradiated seven times, following exponentially increasing irradiation times (90, 380, 900, 1,800, 3,600, 7,200 and 14,400 s). During each irradiation step, the output of the X-ray gun was recorded, which allows the accurate calculation of the dose rate received by the sample (for 12/LA/508 and 13/LA/508 with average dose rates of $0.152\,Gy\,s^{-1}$ and $0.254\,Gy\,s^{-1}$, respectively). Isotropic and baseline corrections were applied uniformly across the measured spectra. The amount of NOCORs in the natural signal was estimated for potential correction (for more details see ref. 69). D_e values were obtained by fitting a single saturating exponential at the appropriate maximum irradiation dose (D_{max}) following the recommendations for accurate dose–response curve estimation[70] (using 12/LA/508 $D_{max} = 2{,}172$ Gy and 13/LA/508 $D_{max} = 3{,}621$ Gy). U-series/ESR age results were modelled using the Monte-Carlo approach[71].

Bayesian modelling. To evaluate the uncertainties of the integrated dating approach (Extended Data Fig. 10b), Bayesian modelling was performed on all independent age estimates using the OxCal (version 4.2) software[72] available at https://c14.arch.ox.ac.uk/oxcal.html. The analysis incorporated the probability distributions of individual dates, and constraints imposed by stratigraphic relationships and the reported minimum–maximum nature of some of the individual age estimates. Each individual age was included as a Gaussian distribution (with mean and standard deviation defined by the age estimate and their associated uncertainties). The U-series profiling ages on the fossil *Pongo* and siamang gibbon teeth yielded a range of dates (80–75 kyr old) and these were incorporated as a uniform distribution over this interval. The age of the breccia deposit was conservatively estimated as the boundary age between the overlying calcite deposits and the age estimates from within the breccia deposit, incorporating all of the constraints described above (Extended Data Fig. 10b).

Data availability. The data that support the findings of this study are available from the corresponding author upon reasonable request.

30. Weidenreich, F. The dentition of *Sinanthropus pekinensis:* a comparative odontography of the hominids (China Geological survey Palaeontologia sinica, new series D, 1937).
31. Moorrees, C. F. A. *The Aleut Dentition* (Harvard Univ. Press, 1957).
32. Rasband, W. S. ImageJ. http://rsb.info.nih.gov/ij/ (National Institutes of Health, USA, 1997–2008).
33. Turner, C. G., Nichol, C. R. & Scott, G. R. In *Advances in Dental Anthropology* (eds Kelley, M. A. & Larsen, C. S.) 13–31 (Wiley-Liss, 1991).
34. Smith, T. M., Olejniczak, A. J., Reid, D. J., Ferrell, R. J. & Hublin, J.-J. Modern human molar enamel thickness and enamel–dentine junction shape. *Arch. Oral Biol.* **51,** 974–995 (2006).
35. Smith, T.M. *et al.* Dental tissue proportions in fossil orangutans from mainland Asia and Indonesia. *Hum. Origins Res.* **1,** e1 (2011).
36. Smith, T. M., Kupczik, K., Machanda, Z., Skinner, M. M. & Zermeno, J. P. Enamel thickness in Bornean and Sumatran orangutan dentitions. *Am. J. Phys. Anthropol.* **147,** 417–426 (2012).
37. Martin, L. B. *Relationships of the later Miocene Hominoidea.* PhD thesis, Univ. College London (1983).
38. Martin, L. Significance of enamel thickness in hominoid evolution. *Nature* **314,** 260–263 (1985).
39. Skinner, M. M., Gunz, P., Wood, B. A. & Hublin, J.-J. Enamel–dentine junction (EDJ) morphology distinguishes the lower molars of *Australopithecus africanus* and *Paranthropus robustus*. *J. Hum. Evol.* **55,** 979–988 (2008).
40. Skinner, M. M., Gunz, P., Wood, B. A., Boesch, C. & Hublin, J. J. Discrimination of extant *Pan* species and subspecies using the enamel–dentine junction morphology of lower molars. *Am. J. Phys. Anthropol.* **140,** 234–243 (2009).
41. Huntley, D. J., Godfrey-Smith, D. I. & Thewalt, M. L. W. Optical dating of sediments. *Nature* **313,** 105–107 (1985).
42. Westaway, K. E. & Roberts, R. G. A dual-aliquot regenerative-dose protocol (DAP) for thermoluminescence (TL) dating of quartz sediments using the light-sensitive and isothermally stimulated red emissions. *Quat. Sci. Rev.* **25,** 2513–2528 (2006).
43. Spooner, N. A. & Franklin, A. D. Effect of the heating rate on the red TL of quartz. *Radiat. Meas.* **35,** 59–66 (2002).
44. Murray, A. S. & Mejdahl, V. Comparison of regenerative-dose single-aliquot and multiple-aliquot (SARA) protocols using heated quartz from archaeological sites. *Quat. Sci. Rev.* **18,** 223–229 (1999).
45. Huot, S., Buylaert, J.-P. & Murray, A. S. Isothermal thermoluminescence signals from quartz. *Radiat. Meas.* **41,** 796–802 (2006).
46. Murray, A. S. & Wintle, A. G. Luminescence dating of quartz using an improved single-aliquot regenerative-dose protocol. *Radiat. Meas.* **32,** 57–73 (2000).
47. Morwood, M. J. *et al.* Archaeology and age of a new hominin from Flores in eastern Indonesia. *Nature* **431,** 1087–1091 (2004).
48. Thomsen, K. J., Murray, A. S., Jain, M. & Botter-Jensen, L. Laboratory fading rates of various luminescence signals from feldspar-rich sediment extracts. *Radiat. Meas.* **43,** 1474–1486 (2008).
49. Murray, A. S., Buylaert, J. P., Thomsen, K. J. & Jain, M. The effect of preheating on the IRSL signal from feldspar. *Radiat. Meas.* **44,** 554–559 (2009).
50. Thiel, C. *et al.* Luminescence dating of the Stratzing loess profile (Austria)—testing the potential of an elevated temperature post-IR IRSL protocol. *Quat. Int.* **234,** 23–31 (2011).
51. Thomsen, K. J., Murray, A. S. & Jain, M. Stability of IRSL signals from sedimentary K-feldspar samples. *Geochronometria* **38,** 1–13 (2011).
52. Buylaert, J. P., Murray, A. S., Thomsen, K. J. & Jain, M. Testing the potential of an elevated temperature IRSL signal from K-feldspar. *Radiat. Meas.* **44,** 560–565 (2009).
53. Stokes, S. *et al.* Alternative chronologies for Late Quaternary (Last Interglacial–Holocene) deep sea sediments via optical dating of silt-sized quartz. *Quat. Sci. Rev.* **22,** 925–941 (2003).
54. Mejdahl, V. Thermoluminescence dating: beta-dose attenuation in quartz grains. *Archaeometry* **21,** 61–72 (1979).
55. Feathers, J. K. & Migliorini, E. Luminescence dating at Katanda—a reassessment. *Quat. Sci. Rev.* **20,** 961–966 (2001).
56. Huntley, D. J. & Baril, M. R. The K content of the K-feldspars being measured in optical dating or in thermoluminescence dating. *Anc. TL* **15,** 11–13 (1997).
57. Huntley, D. J. & Hancock, R. G. V. The Rb contents of the K-feldspars being measured in optical dating. *Anc. TL* **19,** 43–46 (2001).
58. Prescott, J. R. & Hutton, J. T. Cosmic-ray contributions to dose rates for luminescence and ESR dating: large depths and long-term time variations. *Radiat. Meas.* **23,** 497–500 (1994).

59. Zhao, J.-x., Hu, K., Collerson, K. D. & Xu, H.-k. Thermal ionization mass spectrometry U-series dating of a hominid site near Nanjing, China. *Geology* **29,** 27–30 (2001).
60. Zhou, H. Y., Zhao, J. X., Wang, Q., Feng, Y. X. & Tang, J. Speleothem-derived Asian summer monsoon variations in Central China during 54–46 ka. *J. Quat. Sci.* **26,** 781–790 (2011).
61. Clark, T. R. *et al.* Discerning the timing and cause of historical mortality events in modern *Porites* from the Great Barrier Reef. *Geochim. Cosmochim. Acta* **138,** 57–80 (2014).
62. Ludwig, K. R. *User's Manual for Isoplot 3.75. A Geochronological Toolkit for Microsoft Excel* (Berkeley Geochronology Center Special Publication No. 5, 2012).
63. Cheng, H. *et al.* The half-lives of uranium-234 and thorium-230. *Chem. Geol.* **169,** 17–33 (2000).
64. Eggins, S. M. *et al. In situ* U-series dating by laser-ablation multi-collector ICPMS: new prospects for Quaternary geochronology. *Quat. Sci. Rev.* **24,** 2523–2538 (2005).
65. Grün, R., Eggins, S., Kinsley, L., Moseley, H. & Sambridge, M. Laser ablation U-series analysis of fossil bones and teeth. *Palaeogeogr. Palaeoclimatol. Palaeoecol.* **416,** 120–167 (2014).
66. Grün, R. *et al.* ESR and U-series analyses of teeth from the palaeoanthropological site of Hexian, Anhui Province, China. *J. Hum. Evol.* **34,** 555–564 (1998).
67. Ludwig, K. R. *User's Manual for Isoplot 3.00* (Berkeley Geochronology Center, 2003).
68. Joannes-Boyau, R. Detailed protocol for an accurate non-destructive direct dating of tooth enamel fragment using electron spin resonance. *Geochronometria* **40,** 322–333 (2013).
69. Duval, M. & Grün, R. Are published ESR dose assessments on fossil tooth enamel reliable? *Quat. Geochronol.* **31,** 19–27 (2016).
70. Shao, Q., Bahain, J.-J., Falgueres, C., Dolo, J.-M. & Garcia, T. A new U-uptake model for combined ESR/U-series dating of tooth enamel. *Quat. Geochronol.* **10,** 406–411 (2012).
71. Guérin, G., Mercier, N. & Adamiec, G. Dose–rate conversion factors: update. *Anc. TL* **29,** 5–8 (2011).
72. Bronk Ramsey, C. Radiocarbon calibration and analysis of stratigraphy: the OxCal program. *Radiocarbon* **37,** 425–430 (1995).
73. Xing, S., Martinón-Torres, M., Bermúdez de Castro, J. M., Wu, X. & Liu, W. Hominin teeth from the early Late Pleistocene site of Xujiayao, Northern China. *Am. J. Phys. Anthropol.* **156,** 224–240 (2015).

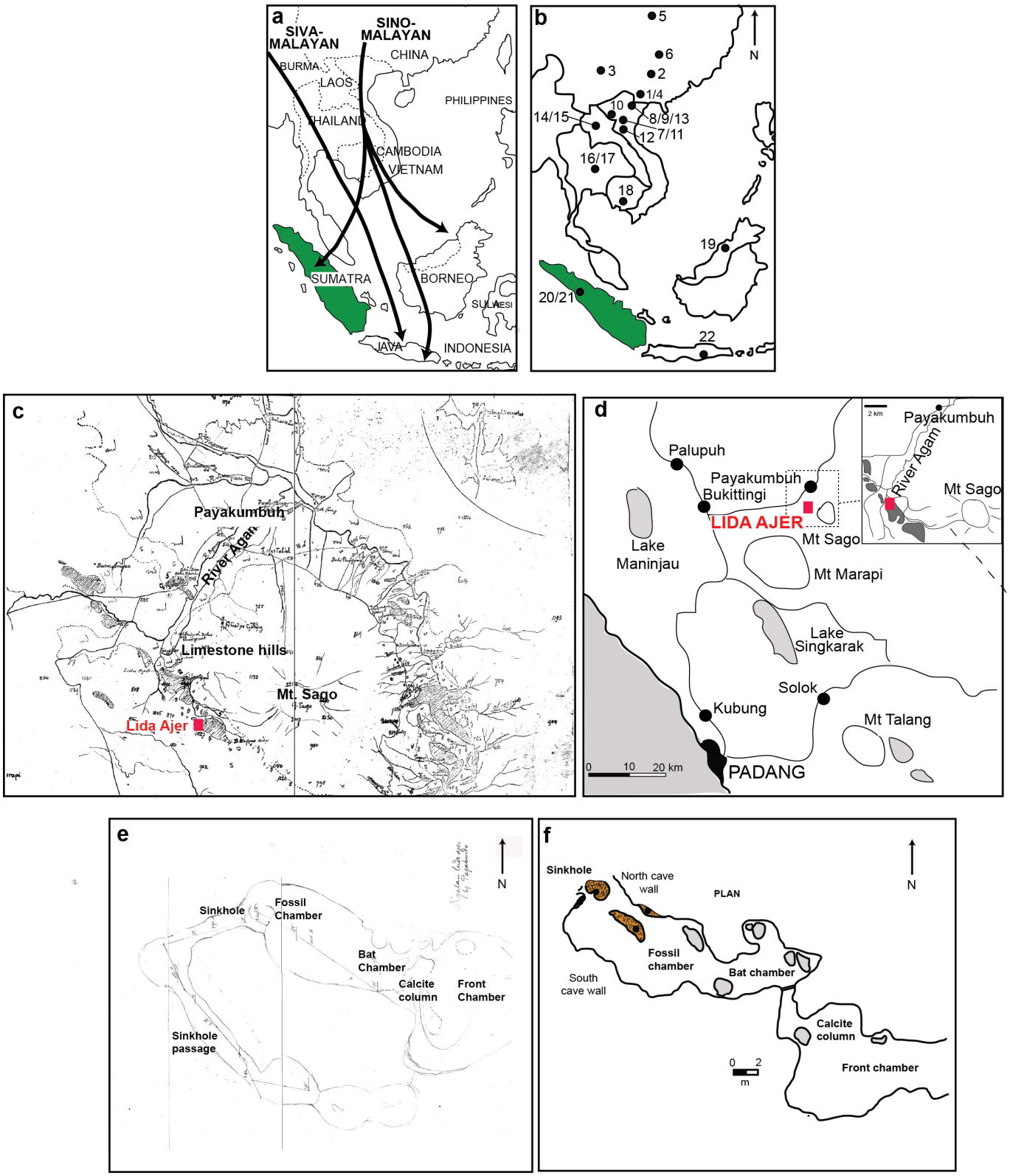

Extended Data Figure 1 | Southeast Asian fossil sites and Dubois' Lida Ajer. a, Corridor of dispersal of fauna into southeast Asia during periods of connection (redrawn with permission from ref. 7). **b**, The main fossil faunal sites in southeast Asia. In southern China: 1, Luijiang; 2, Liucheng; 3, Hoshantung; 4, Hei-Tu'ung; 5, Changyang; 6, Hsing-an. In Vietnam: 7, Lang Trang; 8, Tham Khuyen; 9, Thung Lang; 10, Hang Hum; 11, Ma U 'Oi; 12, Tham Om; 13, Keo Leng. In Laos: 14, Tham Hang; 15, Tham P'a Loi. In Thailand: 16, Thum Wiman Nakin; 17, Thum Phra Khai Phet. In Cambodia: 18, Phnom Loang. In Borneo; 19, Niah Cave. In Indonesia: 20, Lida Ajer; 21, Sibrambang; 22, Punung (redrawn with permission from ref. 7). **c**, Dubois' field sketches of Lida Ajer cave location copied directly from his field notebook—now housed in Leiden (with permission from the Naturalis, the Netherlands). His rough sketch of the cave location close to Payakumbuh village has had annotations added to make the features clearer. **d**, Our map of the cave location for comparison, note the similar relationship between Mount Sago, River Agam and Lida Ajer. **e**, Dubois' plan of the cave, annotations have been added to identify the chambers discussed in the text. **f**, Our plan of the cave for comparison, with the only differences being the absence of the sinkhole passage on our plan (unmapped).

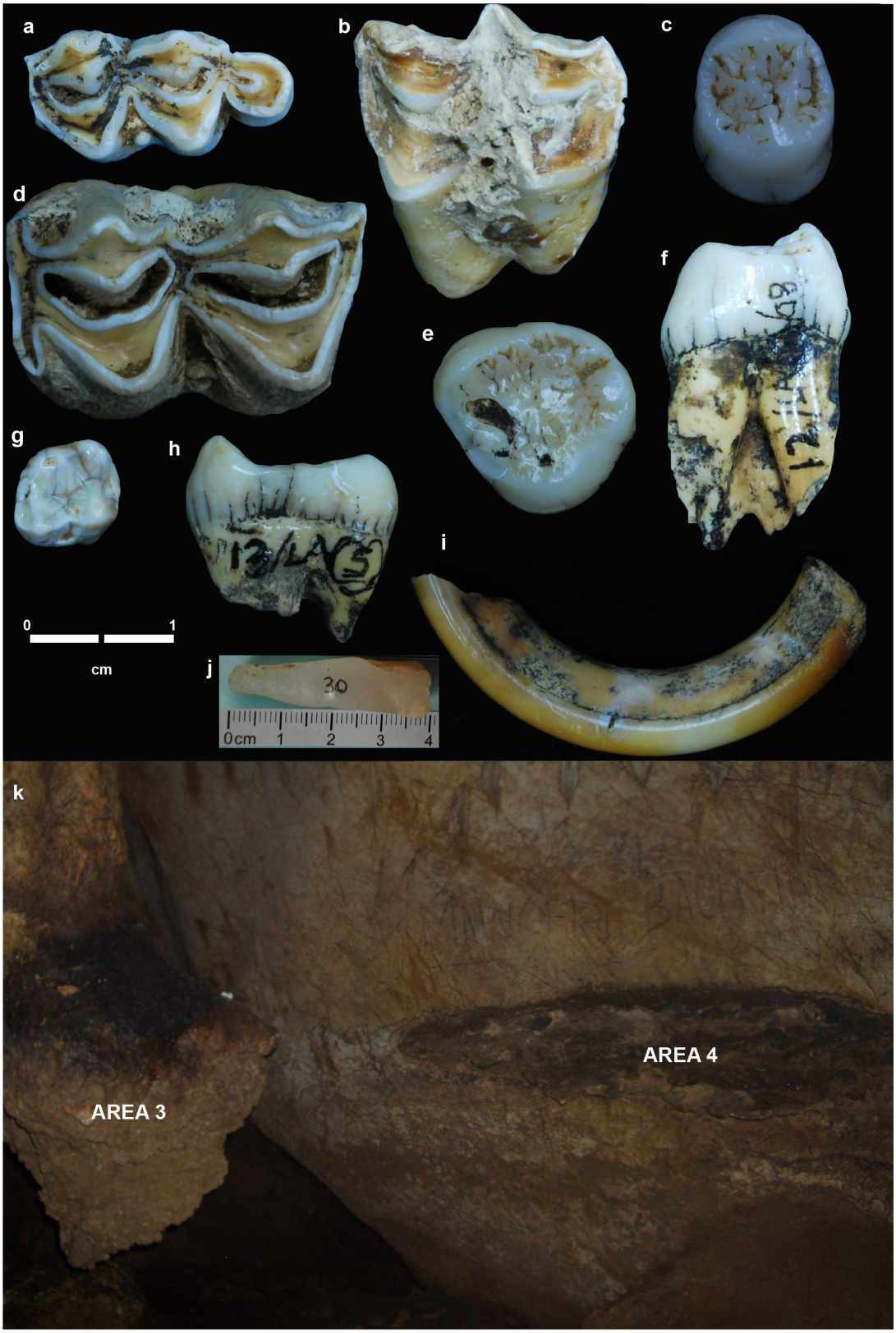

Extended Data Figure 2 | Fauna and speleothems from minor excavations at Lida Ajer in 2007. a, Cervid sp. **b**, Cervid sp. **c**, *Pongo* sp., upper premolar. **d**, *Rusa* sp. **e**, *Pongo* sp., molar. **f**, *Pongo* sp., molar mesial view from **c**. **g**, Siamang gibbon, molar. **h**, *Pongo* sp., molar mesial view from **e**. **i**, *Hystrix* sp. **j**, Soda straw stalactite samples LA08-29 (own scale on photograph). **k**, Photograph of areas 3 and 4 in the cave where the majority of fossil fauna were discovered.

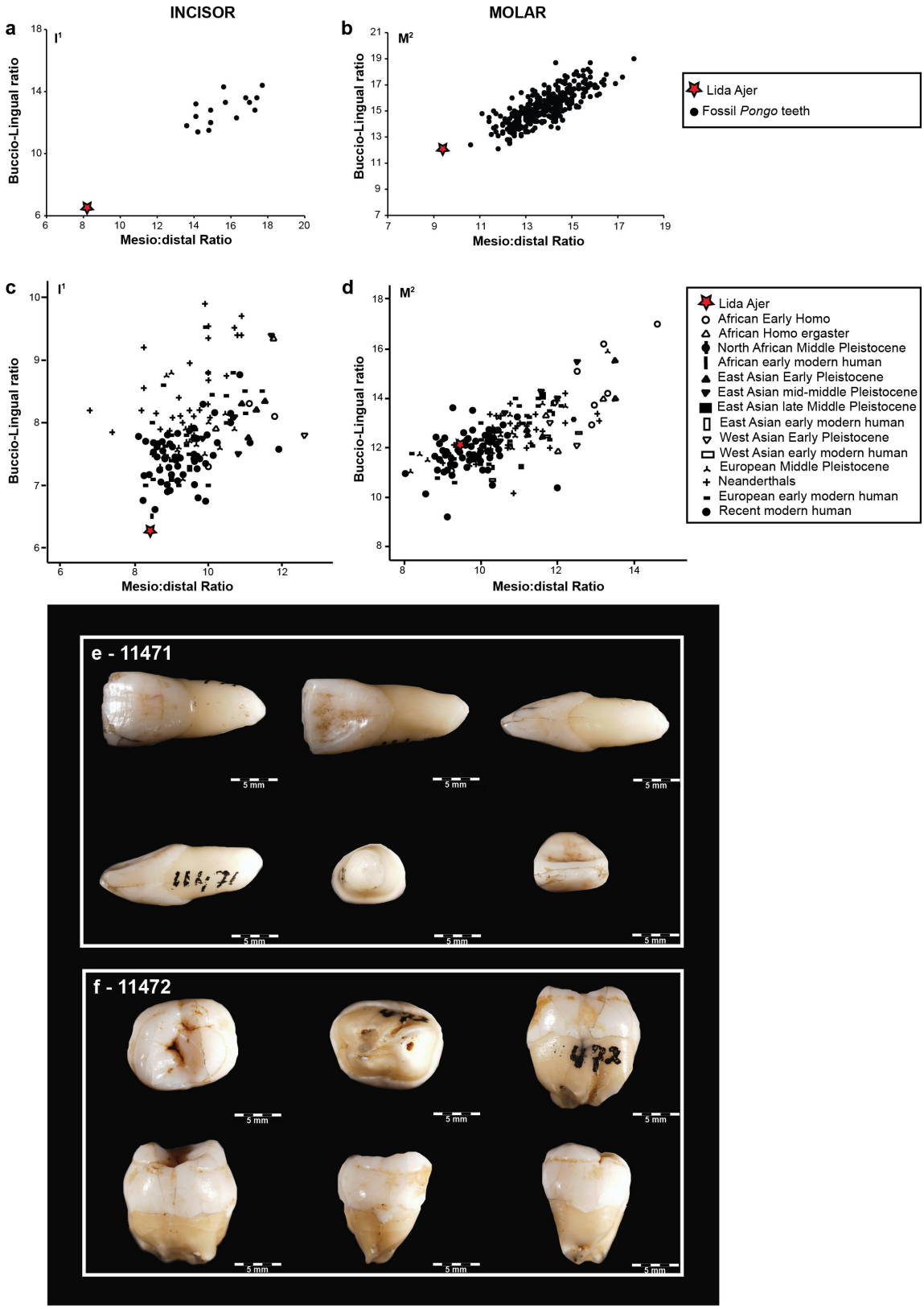

Extended Data Figure 3 | The fossil human teeth from Lida Ajer Cave and associated metrics. a, **b**, The incisor (**a**) and molar (**b**) mesio:distal ratio versus bucco:lingual ratio metrics plotted against data from 37 and 353 fossil *Pongo* teeth[15], respectively. **c**, **d**, The incisor (**c**) and molar (**d**) data are plotted against the full range of *Homo* teeth from African early *Homo* to recent modern (data from ref. 73). In all four plots, the Lida Ajer teeth are denoted by a red star, with the key for symbols in **c**, **d**, representing the different human teeth is indicated on the right. **e**, f, The incisor (**e**) and molar (**f**) from Lida Ajer.

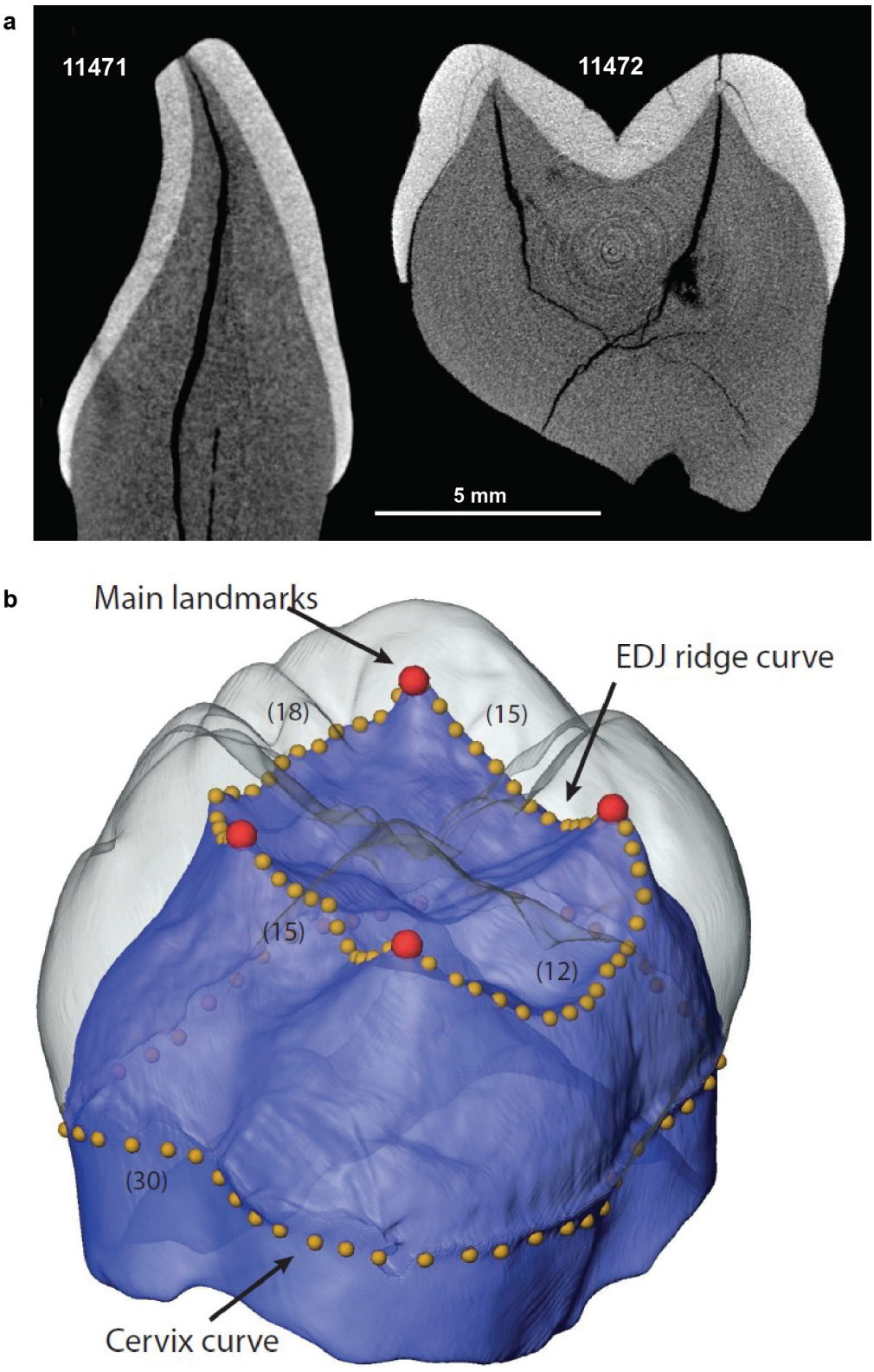

Extended Data Figure 4 | Micro-CT of the Lida Ajer teeth. a, Virtual sections of the Lida Ajer teeth. The labio-lingual section of the incisor is shown on the left, the bucco-lingual section through the mesial molar cusps is shown on the right. Scale bar, 5 mm. **b**, EDJ anatomical landmarks. Landmark protocol for geometric morphometric analysis of EDJ shape. Numbers in brackets represent the number of equidistantly spaced landmarks between main landmarks (red spheres) and around the cervix.

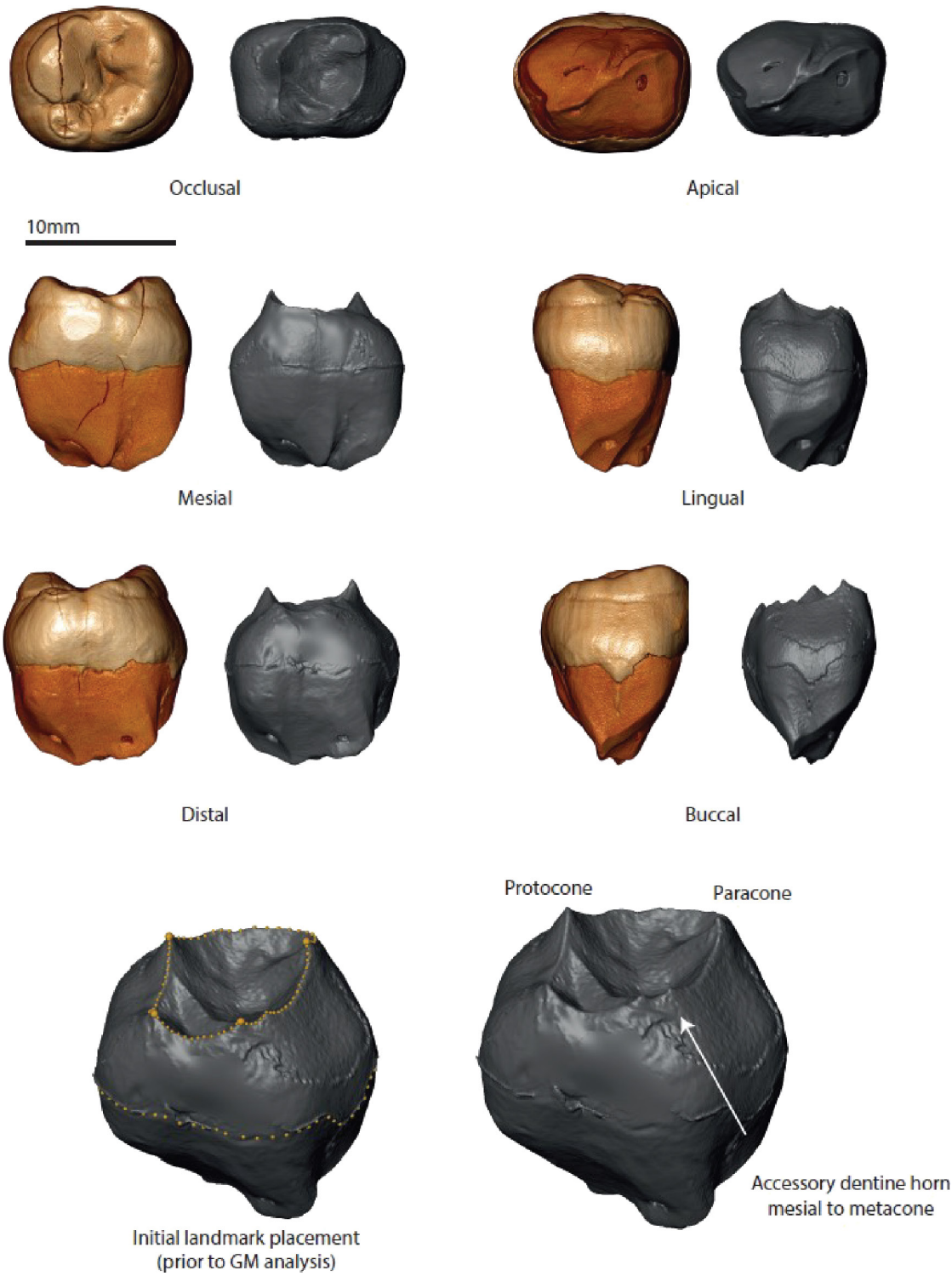

Extended Data Figure 5 | Internal and external structure of the Lida Ajer teeth. Top, CT-based volume renderings of the external surface (left) and surface models of the EDJ (right) of the Lida Ajer molar in six anatomical views. Bottom, initial landmark placement (yellow spheres) capturing the main dentine horns, EDJ ridge and cervix (left) and noting the presence of an accessory dentine horn mesial to the metacone (right).

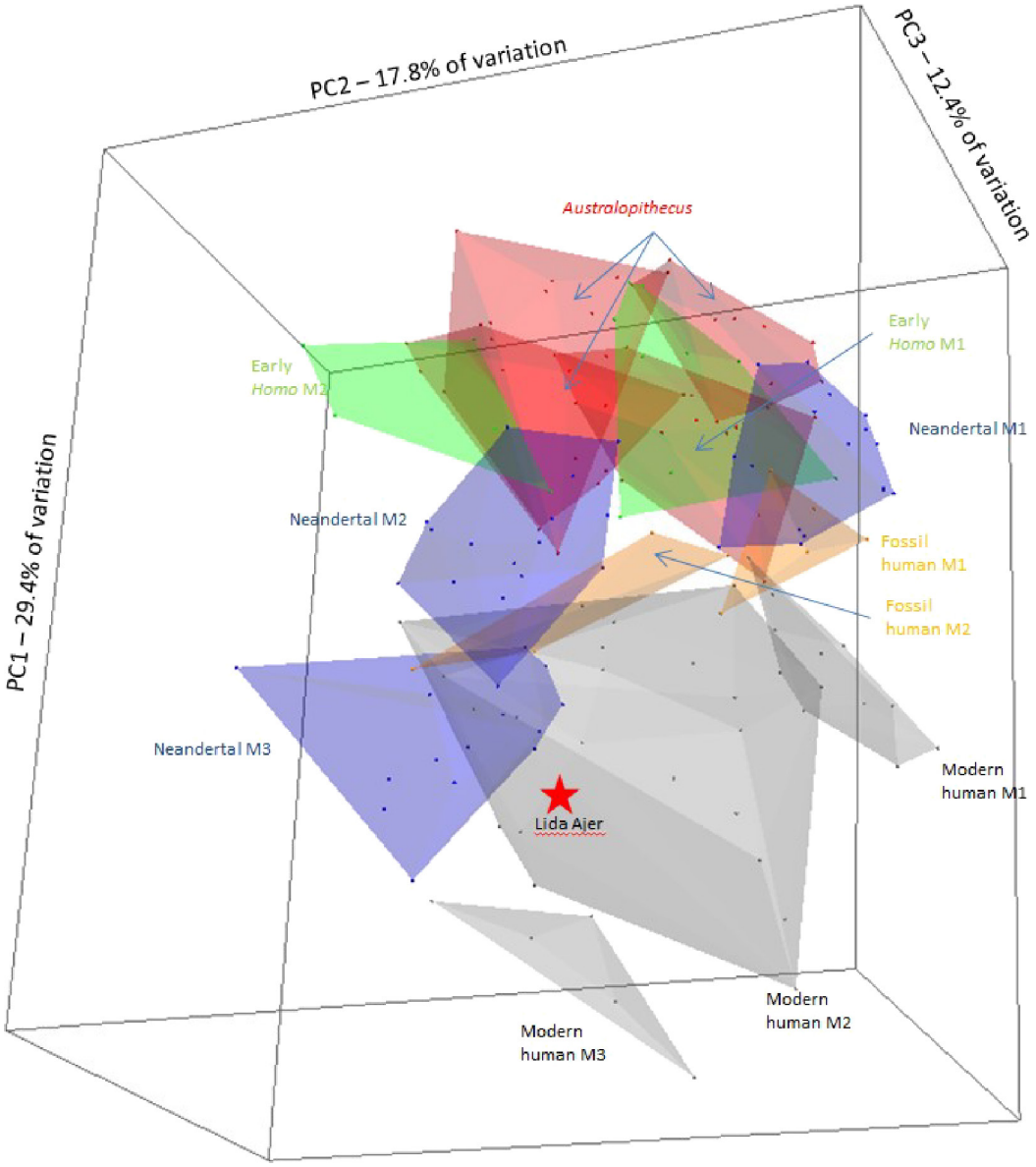

Extended Data Figure 6 | Principal component analysis of the EDJ shape of the comparative sample and the Lida Ajer molar.

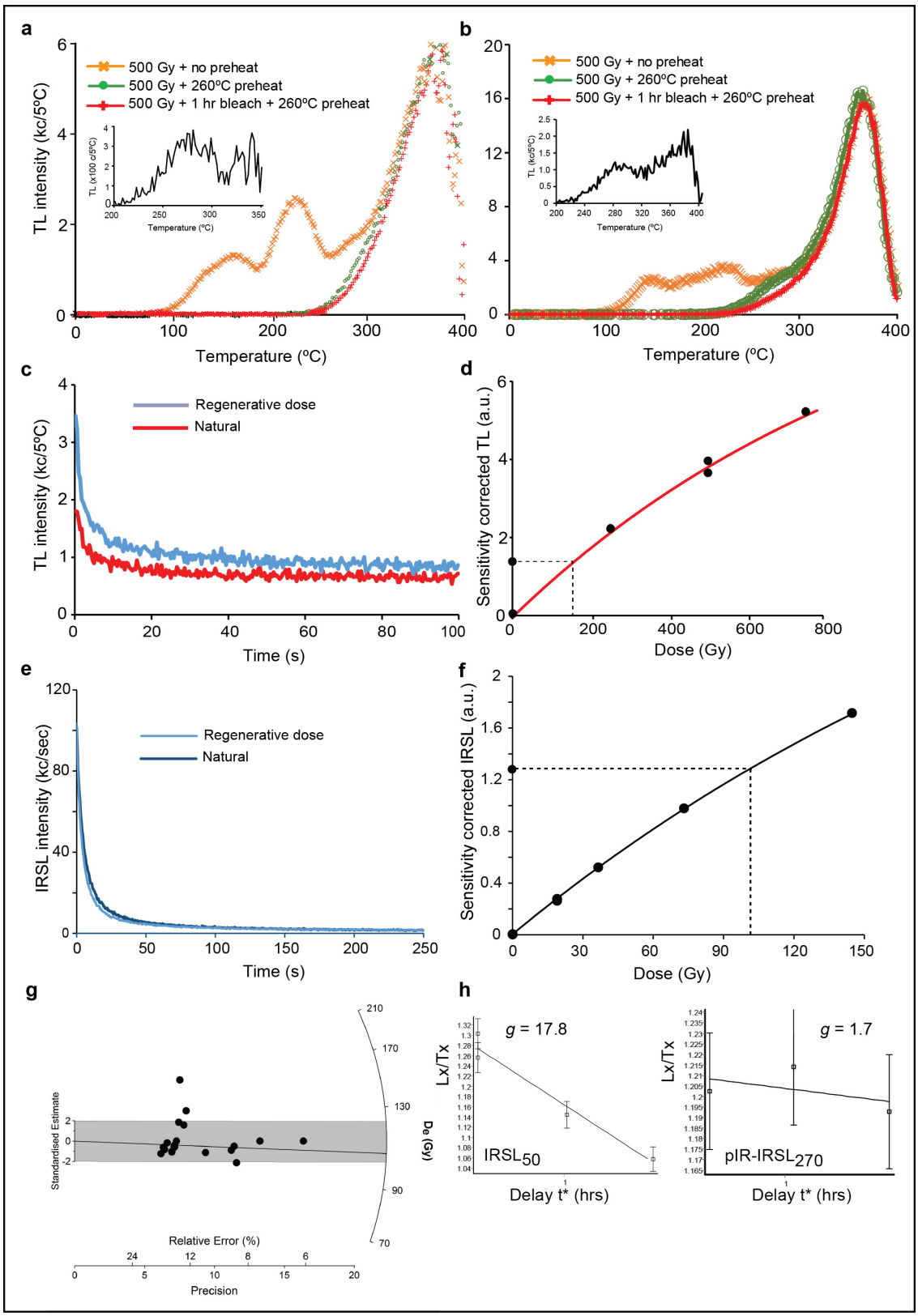

Extended Data Figure 7 | See next page for caption.

Extended Data Figure 7 | Example of the red thermoluminescence and pIR-IRSL data for sample LA-1. a, **b**, A comparison of the red thermoluminescence signal characteristics using glow curves derived from a Liang Bua sample WR1 (**a**) and from the Lida Ajer sample (**b**). The glow curves demonstrate that after 500 Gy dosing the low temperature peaks disappear with the introduction of the 260 °C preheat, and the presence of a light-sensitive shoulder (260–305 °C) that is removed by 1 h of bleaching. The Lida Ajer sample shows similarities with the Liang Bua sample, but has a more defined bleachable shoulder and a more intense signal. **c**, Isothermal decay of the red thermoluminescence signal from sample LA-1. **d**, Dose–response curve for the unbleachable signal derived from aliquot A providing a D_e of 132 ± 13 Gy (see ref. 42 for further methodological details). **e**, pIR-IRSL intensity and shine down from red-diode stimulation for 250 s at 270 °C, displaying the natural curve and a regenerative dose for comparison. **f**, pIR-IRSL sensitivity corrected dose–response providing a D_e of 103 ± 9 Gy. **g**, The D_e values of the 22 aliquots of feldspars plotted on a radial plot. Each aliquot was corrected for minor fading and residual dose and was plotted producing an overdispersion of 17.6%. Prior to running the minimum age model a value of 10% was added to the errors as an estimation of inherent overdispersion within the grains. This was determined by estimating the distribution of D_e values of 12 aliquots after a 4 h bleaching period in a solar simulator. The minimum age model produced a D_e of 105 ± 3 Gy as depicted by a solid black line, which lies within $\pm 10\%$ of the Central age (shaded box), owing to the low overdispersion. This produces an age estimate of 62 ± 5 kyr. **h**, Fading tests for the Lida Ajer feldspars comparing the IR_{50} measurement with a g value of 17.67 with the pIR-$IRSL_{270}$ measurement, which has reduced the g value to 1.74.

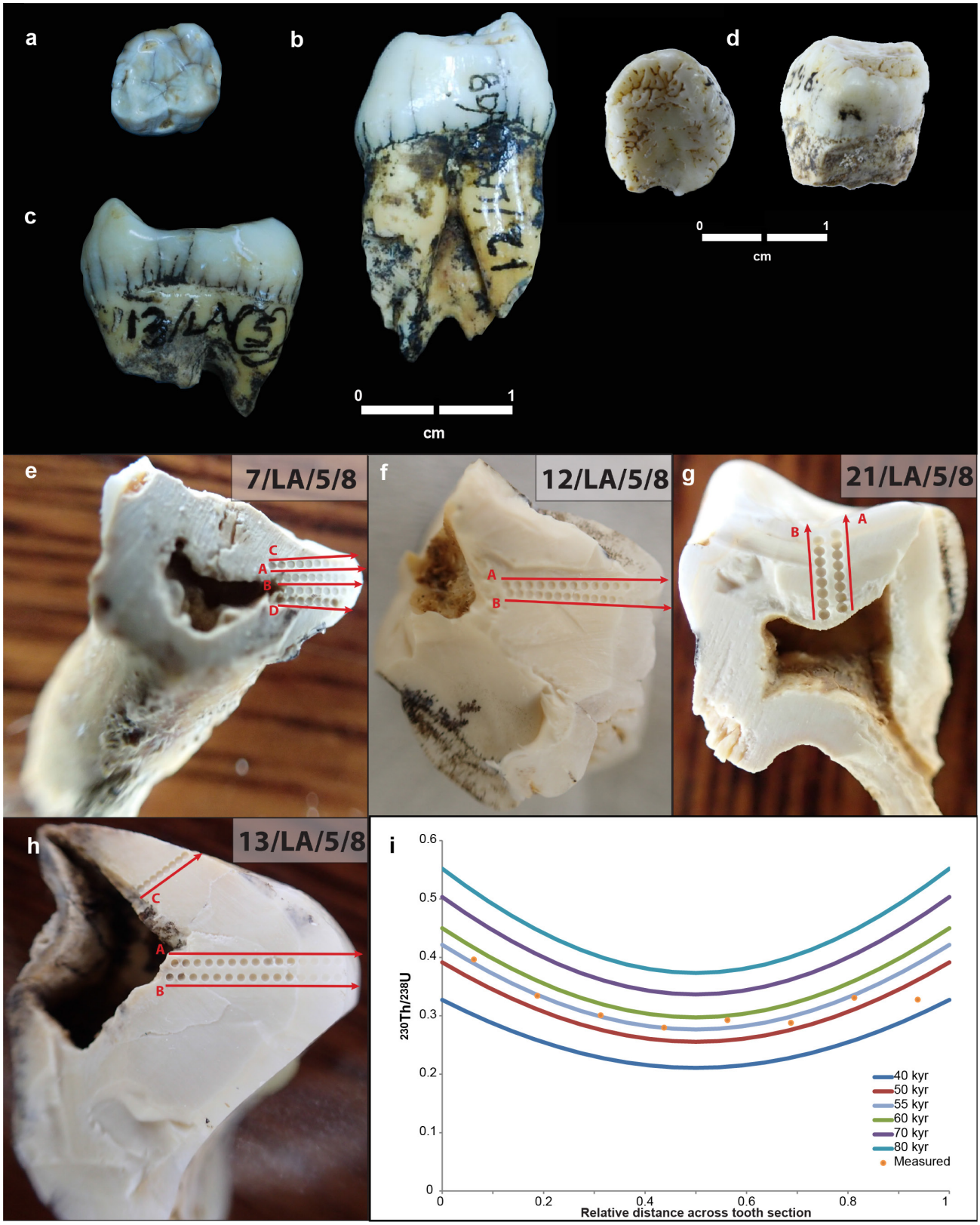

Extended Data Figure 8 | The fossil faunal teeth from Lida Ajer sampled for U-series dating. a, 7/LA/5/08, a molar of siamang gibbon sp., sampled during our excavations. **b**, Sample 12/LA/5/08, a premolar of *Pongo* sp., sampled during our excavations. **c**, 13/LA/5/08, a molar of *Pongo* sp., sampled during our excavations. **d**, Dubois 9967A, a *Pongo* sp. molar from Dubois's original excavation—borrowed from the Naturalis Museum in the Netherlands. **e–h**, U-series profiling tracks on the 4 fossil teeth (7-, 12-, 13-, and 21/LA/5/08). **i**, Example of the best fit D–A (diffusion–absorption model) date profile for sample 13/LA/5/08 (with $4/8 = 1.066$, $t' = 1.0$) demonstrating that the age estimate fits the model at around 55 kyr. The possibility of delayed uptake of uranium and the absence of evidence for uranium leaching means that this should be treated as a minimum age. The U-series profiles from other teeth did not fit well with the predictions of the D–A model owing to complex U-uptake (and potentially U-loss) processes in the sampled teeth.

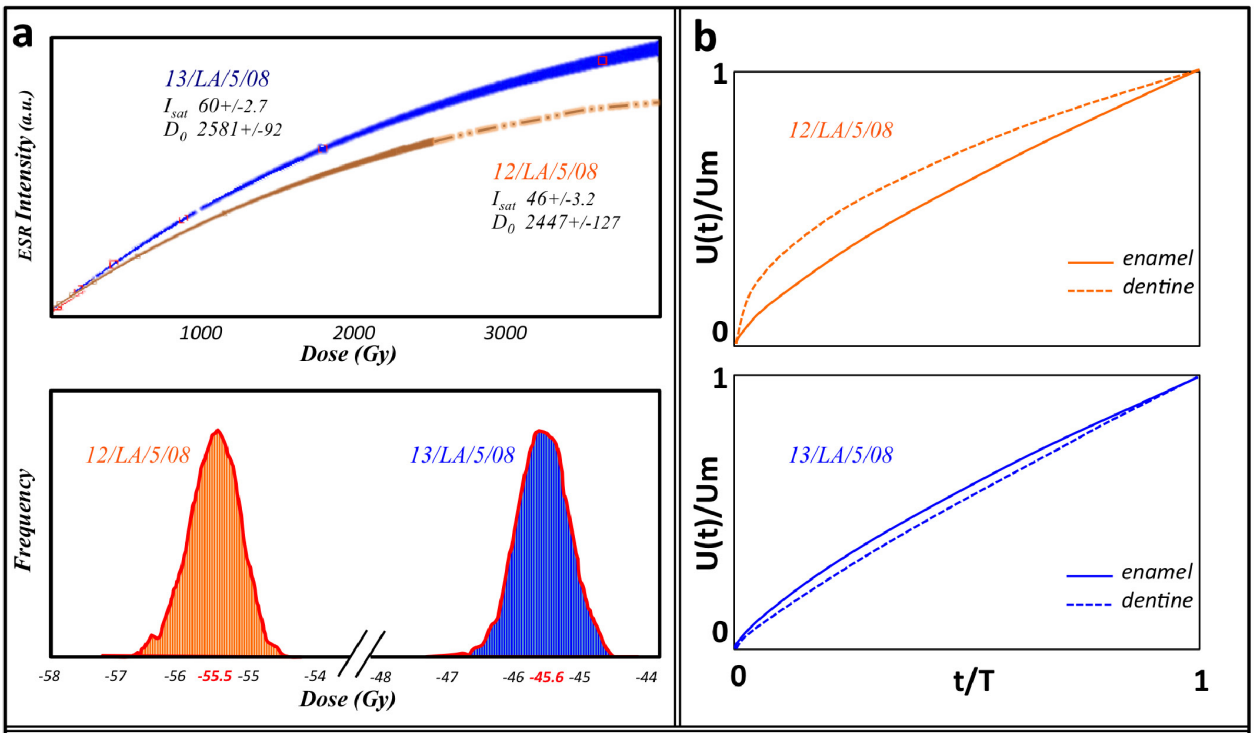

c

Sample	Dental Tissue	U (ppm)	2-s error	U/Th	$^{230}Th/^{234}U$	2-s error	$^{234}U/^{238}U$	2-s error	Age (ka)	2-s error
12/LA/5/08	Enamel	1.05	0.21	42	0.3471	0.3	3.2542	0.05	-	-
	Dentine	6.52	0.97	42581	0.3835	0.05	1.0652	0.05	**41.2**	**2.6**
13/LA/5/08	Enamel	**0.82**	0.68	**28**	0.3051	0.3	3.8588	0.05	-	-
	Dentine	9.25	0.49	81189	0.2840	0.05	1.0597	0.05	**48.4**	**5.3**

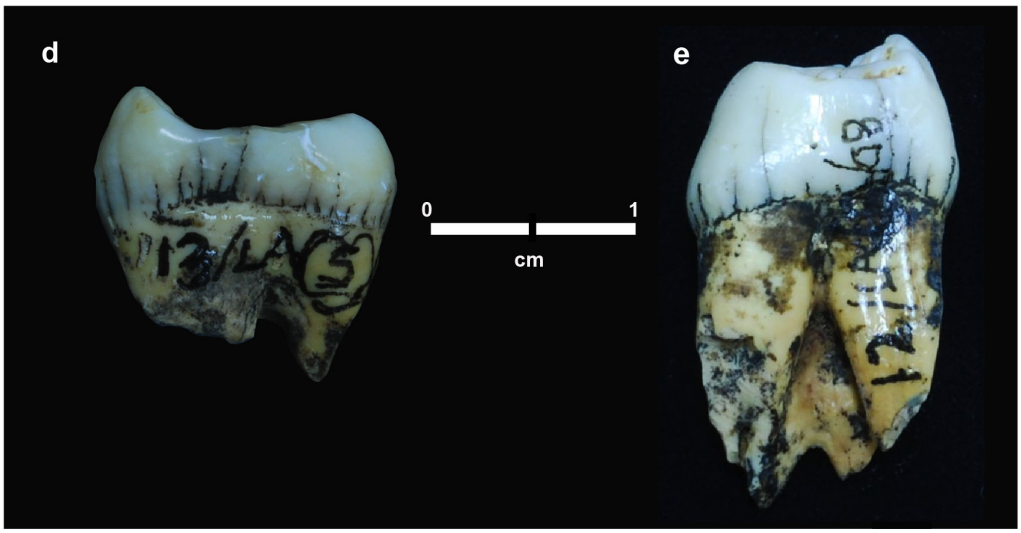

Extended Data Figure 9 | ESR dating of two Fossil *Pongo* teeth 12/LA/5/08 (orange) and 13/LA/5/08 (blue). a, ESR dose equivalent (D_e) calculation. Top, Markov Chain Monte-Carlo fitted dose–reponse curve for each of the samples, using McDoseE 2.0 with a single saturating exponential function and 100,000 iterations. Bottom, ESR dose equivalent distribution of the Markov Chain Monte-Carlo model with McDoseE 2.0. **b**, Uranium uptake model in the different tissues used for the U-series/ESR age calculation. **c**, Table summarizing the U-series values (averaged) obtained by LA-MC-ICPMS on the ESR fragment and dentine directly in contact (EDJ) and used in the coupled U-series/ESR age model. No ages were calculated for U concentration <1 p.p.m. or U/Th ratio <500. **d**, Sample 13/LA/5/08. **e**, Sample 12/LA/5/08.

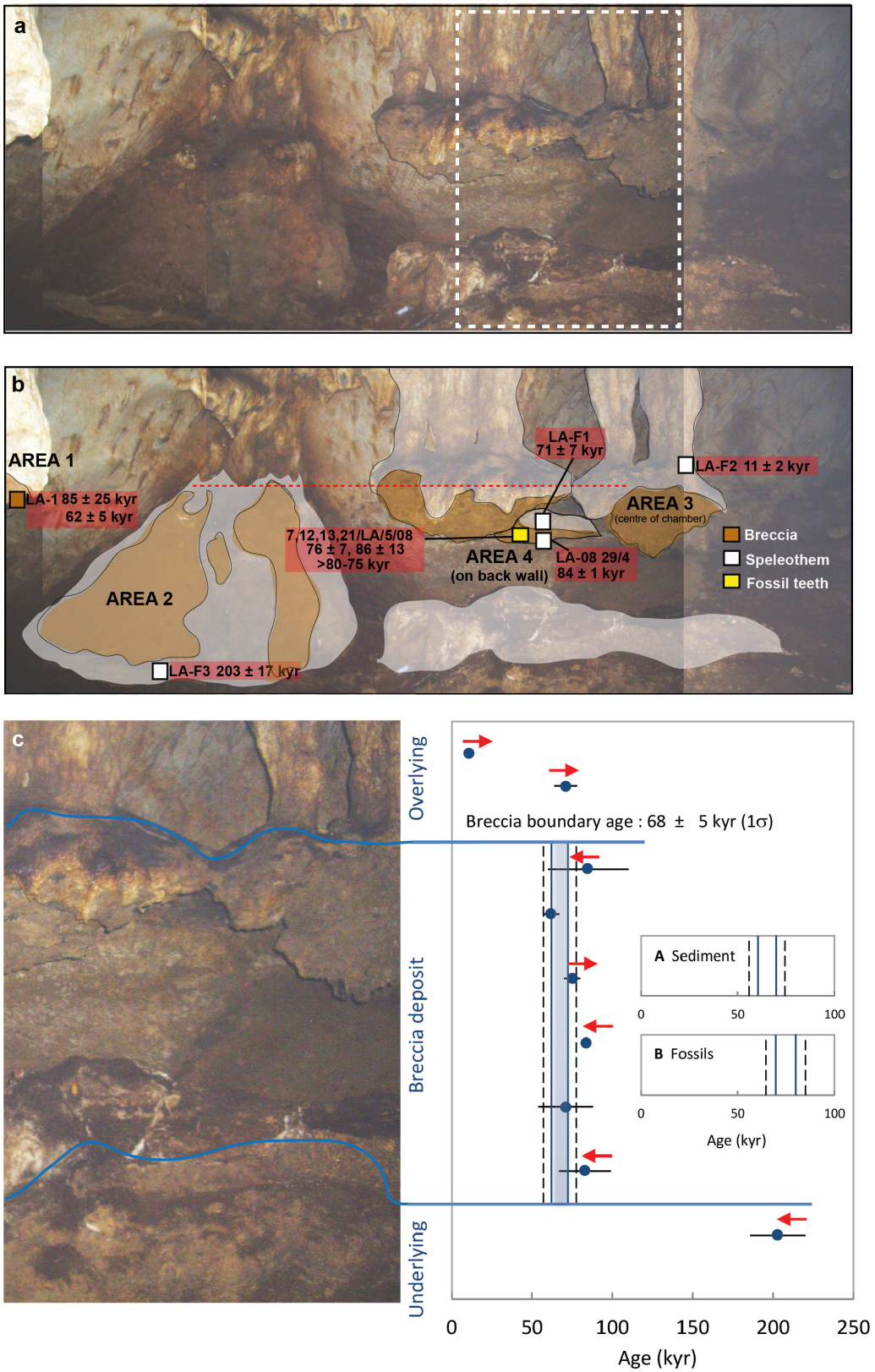

Extended Data Figure 10 | Lida Ajer fossil chamber; new modelled chronology. a, Photograph of the fossil chamber, showing the location and structure of the breccia and flowstone units. **b**, Annotated photograph of the fossil chamber with the sampling locations and dating results found in Supplementary Tables 7, 8, 11. **c**, Bayesian analysis of the red thermoluminescence, U-series and coupled U-series/ESR dating results to construct the new modelled chronology for Lida Ajer. The photograph on the left (taken from the dashed box in **a**) depicts the boundaries between the underlying flowstone, the breccia deposit and overlying flowstone units. Note: the red thermoluminescence and ESR error on the age estimates are presented at 1σ, while the U-series errors have been presented at 2σ. The main figure uses all the available data, while inset A uses only the breccia data (from the red thermoluminescence and pIR-IRSL dating of the breccia matrix and U-series dating of the flowstones and soda straw) and inset B uses only the fossil tooth data (from U-series age depth modelling and coupled U-series/ESR dating of the teeth directly).